Inspection tools for Gaussian Process Regression Modeling of Electromagnetic Fields of Electronic Boards and Chips

Tomas Monopoli
DEIB
Politecnico di Milano
Milan, Italy
tomas.monopoli@polimi.it

Xinglong Wu
DEIB
Politecnico di Milano
Milan, Italy
xinglong.wu@polimi.it

Sergio A. Pignari
DEIB
Politecnico di Milano
Milan, Italy
sergio.pignari@polimi.it

Johannes Wolf
TEC-EP
ESA/ESTEC
Noordwijk, Netherlands
Johannes.Wolf@esa.int

Flavia Grassi
DEIB
Politecnico di Milano
Milan, Italy
flavia.grassi@polimi.it

***Abstract*—Gaussian Process Regression (GPR) has emerged as a powerful technique for building surrogate models of electromagnetic field scans in electronic systems. However, standard GPR models often struggle to capture the non-isotropic and complex spatial patterns commonly found in electronic board field distributions. In this paper, we propose some inspection tools to analyze the underlying correlation structure in the measurement data. This analysis is demonstrated by considering as input data the near field emissions from a bent miscrostrip line (full-wave simulations) and a chip (near-field measurements).**

***Index Terms*—Gaussian Process Regression, Near-field scanning, Printed circuit boards (PCB), Integrated Circuit (IC).**

I. Introduction

The recent trend in miniaturization and high clock frequencies has enabled greater performance in modern chips and Printed Circuit Boards (PCBs), but worsened the overall Electromagnetic Compatibility (EMC) profile. It has therefore become more important to properly characterize the electromagnetic behavior of the single board in order to ensure its compatibility with larger systems. To achieve this, a number of radiated emission tests employing near-field (NF) probes have been explored [1], [2]. Indeed, NF techniques are gaining increasing attention for EMC pre-compliance assessment [3], [4]. Focusing on the characterization of the Device Under Test (DUT) emissions, NF probes are widely employed to map the field distribution [3].

After a NF measurement, an array of sample point locations X and sample point values y is collected. In practice, the measured values do not correspond exactly with the value of the physical field due to measurement noise, positioning uncertainty and so on. The extraction of a field estimate from noisy data is called *surrogate model* extraction. The topic of efficient surrogate model extraction has garnered attention in the EMC community both for modeling of fields radiated by electronic boards [5] and in building efficient adaptive sampling techniques [6]. The most popular surrogate model extraction method is Gaussian Process Regression (GPR) [7].

However, applying the standard GPR models to electromagnetic field scans of electronic boards presents challenges. Indeed, highly localized fields, sharp gradients, and anisotropic patterns can limit the effectiveness of standard GPR models. This paper investigates the applicability of GPR to collected measurements. For this purpose, some new inspection tools based on correlation matrix analysis are proposed to highlight the correlation structure of the NF measurement data.

The remainder of this paper is organized as follows. Section 2 provides an overview of GPR, Section 3 highlights the limitations of standard models for electronic boards, Section 4 introduces the correlation analysis technique. Finally, Section 6 concludes the paper.

II. Gaussian Process Regression for Electromagnetic Field Scans

GPR is a powerful non-parametric Bayesian approach for modeling and predicting complex functions from limited observations [7]. In the context of electromagnetic field scans, GPR can be used to construct surrogate models that approximate the fields based on a set of measured samples.

A. Brief Overview of GPR

A Gaussian Process (GP) is a collection of random variables, any finite number of which have a joint Gaussian distribution. In GPR, the target function $f(\mathbf{x})$ is modeled as a

This work was supported by the European Space Agency (ESA-ESTEC) under Grant ESA RFP/3-17397/21/NL/GLC/my

realization of a GP with mean function $m(\mathbf{x})$ and covariance function (kernel) $k(\mathbf{x}, \mathbf{x}')$:

$$f(\mathbf{x}) \sim \mathcal{GP}(m(\mathbf{x}), k(\mathbf{x}, \mathbf{x}')) \tag{1}$$

Given a set of training data $\mathcal{D} = \{(\mathbf{x}_i, y_i)\}_{i=1}^N$, where $\mathbf{x}_i$ are input points and y_i are corresponding target values, GPR aims to predict the function value f_* at a new input point $\mathbf{X}^* = \{\mathbf{x}_*\}$. The joint distribution of the training targets $\mathbf{y}$ and the predicted value f_* is given by:

$$\begin{bmatrix} \mathbf{y} \\ \mathbf{f}_* \end{bmatrix} \sim \mathcal{N}\left(\begin{bmatrix} \mathbf{m} \\ \mathbf{m}_* \end{bmatrix}, \begin{bmatrix} \mathbf{K}_{\mathbf{X},\mathbf{X}} & \mathbf{K}_{\mathbf{X},*} \\ \mathbf{K}_{\mathbf{X},*}{}^T & \mathbf{K}_{*,*} \end{bmatrix} \right) \tag{2}$$

where $\mathbf{m}$ is the mean vector of the training points, $\mathbf{m}_*$ is the mean of the test point, $\mathbf{K}_{\mathbf{X},\mathbf{X}}$ is the covariance matrix of the training points, $\mathbf{K}_{\mathbf{X},*}$ is the covariance vector between the test points and the training points, and $\mathbf{K}_{*,*}$ is the covariance matrix between the test points.

The posterior predictive distribution of f_* given the training data $\mathcal{D}$ is a Gaussian distribution. Assuming the training data is normalized, then $m(x) = 0$, i.e. no bias is assumed as prior knowledge. So, $\mathbf{m}_* = \mathbf{m} = \mathbf{0}$. The expressions of the mean and covariance are given by

$$\mathbb{E}[f_*|\mathcal{D}, \mathbf{X}_*] = \mathbf{K}_{\mathbf{X},*}{}^T \mathbf{K}_{\mathbf{X},\mathbf{X}}{}^{-1} \mathbf{y} \tag{3}$$

$$\mathrm{Cov}[f_*|\mathcal{D}, \mathbf{X}_*] = \mathbf{K}_{*,*} - \mathbf{K}_{\mathbf{X},*}{}^T \mathbf{K}_{\mathbf{X},\mathbf{X}}{}^{-1} \mathbf{K}_{\mathbf{X},*} \tag{4}$$

B. Kernel Functions

The choice of the kernel function $k(\mathbf{x}, \mathbf{x}')$ is a crucial aspect of GPR, as it encodes the prior assumptions about the structure and smoothness of the target function. Kernel functions must be chosen carefully to reflect the underlying characteristics of the data and the desired properties of the surrogate model.

One of the most commonly used kernel functions in GPR is the Radial Basis Function (RBF) kernel. The RBF kernel is defined as:

$$k_{\mathrm{RBF}}(\mathbf{x}, \mathbf{x}') = \sigma^2 \exp\left(-\frac{\|\mathbf{x} - \mathbf{x}'\|^2}{2\ell^2} \right) \tag{5}$$

where σ^2 is the signal variance and ℓ is the characteristic length scale. The RBF kernel is infinitely differentiable, which leads to very smooth function estimates.

The shape of the kernel function depends on the values of ℓ and σ, that are the kernel *hyperparameters*. The length scale parameter ℓ determines the scale at which the function varies. Smaller values of ℓ result in rapidly varying functions, while larger values correspond to smoother functions. The signal variance σ^2 controls the overall magnitude of the function.

C. Kernel Hyperparameters

The kernel hyperparameters play a vital role in determining the behavior and performance of the GPR model. Indeed, they control properties such as smoothness, flexibility, and complexity of the functions that can be modeled by the GP.

One method to determine hyperparameters is to maximize the training data marginal likelihood. This likelihood assesses the model fit to the data and includes a penalty for complexity to avoid overfitting, aligning with Maximum Likelihood Estimation (MLE) principles.

III. Limitations of Standard GPR Models for Electronic Boards

Standard GPR models, such as those based on the widely used Radial Basis Function (RBF) kernel, assume smooth and isotropic field variations. However, electromagnetic field scans of electronic boards often exhibit highly localized fields, sharp gradients and anisotropic patterns. This can limit the effectiveness of standard GPR models.

A. Example Devices

In this paper, we consider NF radiations from two examples of electronic boards.

1) Bent Microstrip Line (MSL): The bent microstrip line is a simple yet representative example of a device that exhibits smooth and isotropic electromagnetic field variations. The bent configuration introduces a controlled level of complexity to the field that serves as a benchmark case to evaluate the performance of standard GPR models. The radiated fields are obtained via full-wave simulation with a superimposed white gaussian noise such that the SNR is set to 20 dB.

2) The integrated circuit (IC): A more complex and realistic example is the PWM microcontroller C2000 F28069 Piccolo Series Board from Texas Instruments (TI), shown in Fig. 1(b). The board is a 4-layer PCB 51×131 mm and a thickness of 1.57 mm.

The scanned region, shown in Fig. 1(b), focuses on the microcontroller unit, that is the chip in the center of the board. This region was scanned at 1 mm height at 270 MHz using

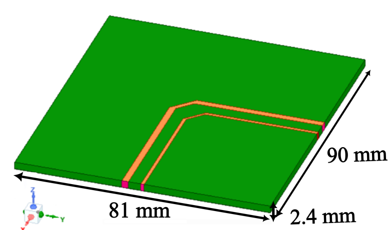

(a)

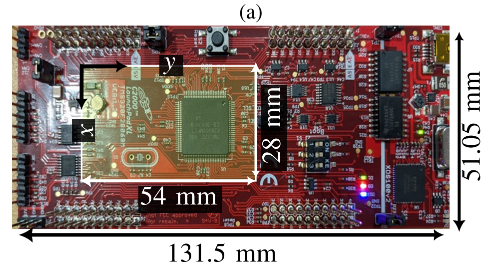

(b)

Figure 1. Example DUTs: (a) virtual bent MSL and (b) view of the IC on the TI Board and of the scanned region.

a RFE04s Langer probe for the E_z component. The radiated field and measurement noise are estimated as sample mean and variance respectively over 20 repeated scans. Note that NF probes return measurements in dBm before being converted to field values. For simplicity field scans are reported here in dBm.

B. Applying Standard GPR

A surrogate model is extracted for both devices using the standard GPR method. For both the example devices the initial values of the hyperparameters are: $\ell = 3$ mm, $\sigma^2 = 0.2$ for the normalized samples $\mathbf{y}$ with range equal to 1. The obtained results are shown in Fig. 2. It can be seen that

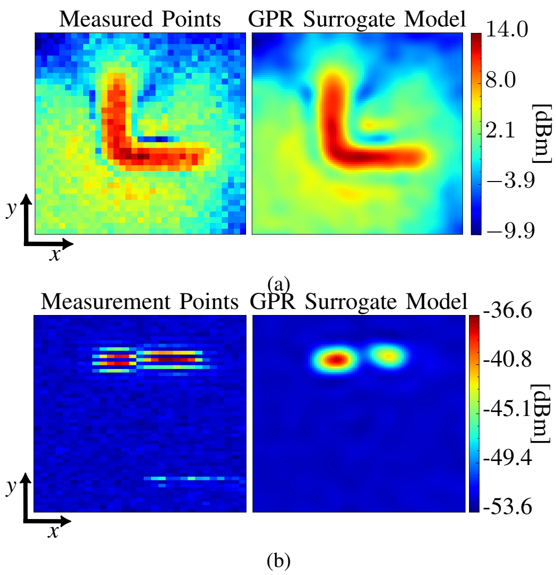

Figure 2. Standard GPR applied to the two example devices: (a) bend MSL and (b) IC.

this approach offers good results for the Bend MSL device, while the surrogate model of the TI board does not reflect the sampled field structure.

The RBF kernel assumes a single length scale parameter ℓ that determines the smoothness of the function in all directions. This isotropic assumption may not hold for electronic board scans, where the field variations can differ significantly along different axes. Moreover, the smoothness assumptions imposed by the RBF kernel may not accurately represent the sharp gradients and discontinuities often present in electronic board field scans. The inability to capture these local features can result in over-smoothing and loss of important details in the surrogate model.

To address these limitations, we propose some tools to inspect the correlation structure of the measurement data.

IV. Correlation Analysis for Electronic Board Field Scans

Correlation analysis is a powerful tool for identifying and quantifying the relationships between variables in a dataset. In the context of electronic board field scans, it can be used to uncover the non-isotropic field characteristics and inform the design of non-standard GPR models. This section introduces the correlation matrix as a means to interpret the field patterns and compares it with variogram analysis, a common technique in geostatistics.

A. Correlation Matrix

The correlation matrix, a symmetric matrix containing pairwise correlation coefficients, provides insights into the relationships between field values at different spatial locations on an electronic board. Pearson's correlation coefficient between locations $\mathbf{x}_i$ and $\mathbf{x}_j$ is given by:

$$\rho_{ij} = \frac{\mathrm{Cov}(f(\mathbf{x}_i), f(\mathbf{x}_j))}{\sqrt{\mathrm{Var}(f(\mathbf{x}_i))\mathrm{Var}(f(\mathbf{x}_j))}} \tag{6}$$

where $\mathrm{Cov}(f(\mathbf{x}_i), f(\mathbf{x}_j))$ is the covariance, and $\mathrm{Var}(f(\mathbf{x}_i))$ and $\mathrm{Var}(f(\mathbf{x}_j))$ are the variances of the field values at the respective locations.

High correlation coefficients between nearby locations indicate smooth and continuous field variations, while low or negative correlations suggest sharp gradients or discontinuities.

Correlation matrices can be constructed by computing (6) on the measured values column by column (x-correlation) and row by row (y-correlation). This results in square matrices with dimensions equal to the number of columns or rows respectively. As the matrices are symmetrical, the upper and lower triangles are combined into a single plot for an overview of the correlation properties. Fig. 3 shows the correlation matrices, with the upper triangle representing y-correlation and the lower triangle representing x-correlation. It should be noted that if the number of rows is different from the number of columns, the upper and lower triangles will have different dimensions, see Fig. 3(b).

B. Interpreting the Correlation Matrix Plots

The correlation matrix provides insights into the spatial structure of the EM field scans. The value at position (i, j) represents the correlation coefficient between the i-th and j-th columns (x-correlation) or rows (y-correlation) of the scan data. The diagonal entries are always 1, as they represent the correlation of each column or row with itself.

The correlation values are typically clipped at 0, resulting in output values between 0 and 1, as negative correlations cannot represent the local regularity of EM fields and so are not of interest for building GPR models. The patterns in the correlation matrix can reveal important characteristics of the field:

- Strong correlation along the diagonal and its vicinity indicates a smooth and continuous field distribution.
- Rapid decay of correlation values away from the diagonal suggests sharp gradients or discontinuities.
- Asymmetric or irregular patterns may indicate anisotropic or non-stationary field variations.
- Irregular decay moving away from the diagonal suggests periodic or clustering behavior.
- Differences in the x-correlation and y-correlation patterns point to anisotropic fields.

In Fig. 3 (a), the bent MSL shows strong correlation along the diagonal and a gradual decay away from it, suggesting

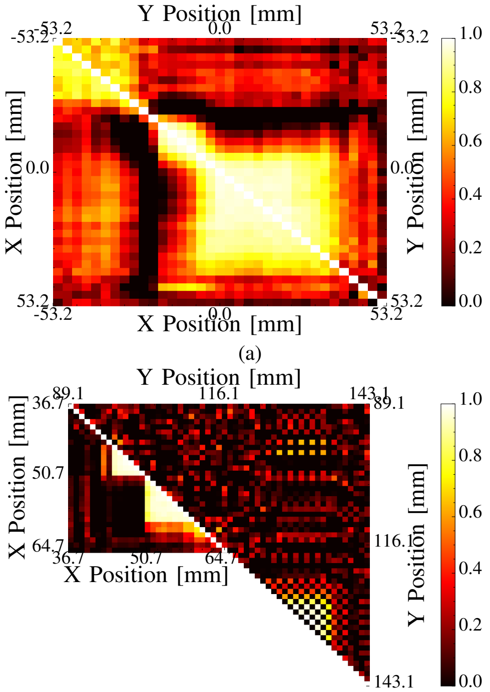

(a)

(b)

Figure 3. Correlation matrices of the two example devices scans: (a) bent MSL and (b) IC. If the sample matrix has a number of rows that is different from the number of columns, the upper and lower triangles will have different dimensions as it can be seen in (b).

a smooth and isotropic field suitable for GPR modeling. In contrast, in Fig. 3 (b), the IC exhibits a more complex correlation structure, with distinct patterns in the x-correlation and y-correlation matrices, indicating anisotropic field variations. The upper triangle shows no smooth correlation structure in the y direction useful for a GPR surrogate model, while the lower triangle reveals a clear correlation structure in the x direction.

C. Comparison with Variogram Analysis

Variogram analysis, a geostatistical technique, offers a more precise estimation of spatial dependence. The variogram measures the semivariance, i.e. half the average squared difference between pairs of observations, as a function of their spatial separation (lag distance). Similarly, the correlogram measures the correlation for each lag distance. Fig. 4 shows the variogram and correlogram for the two test cases under analysis, with angle 0° representing correlation in the x direction and angle 90° representing correlation in the y direction.

Combining insights from correlation and variogram analysis provides a comprehensive understanding of the non-isotropic field characteristics on electronic boards, possibly pointing towards a better sampling strategy.

V. Conclusion

In this paper, we have addressed the limitations of standard GPR models in capturing the non-isotropic and complex spatial patterns often encountered in electronic board's field distributions. A correlation analysis was introduced to identify correlation patterns and non-isotropic behavior in electronic board scans. By examining the correlation matrices and variograms, we gain insights into the spatial structure and dependence of the electromagnetic fields. Future development of this research will be aimed at finding a solution to the limitations explored in this paper.

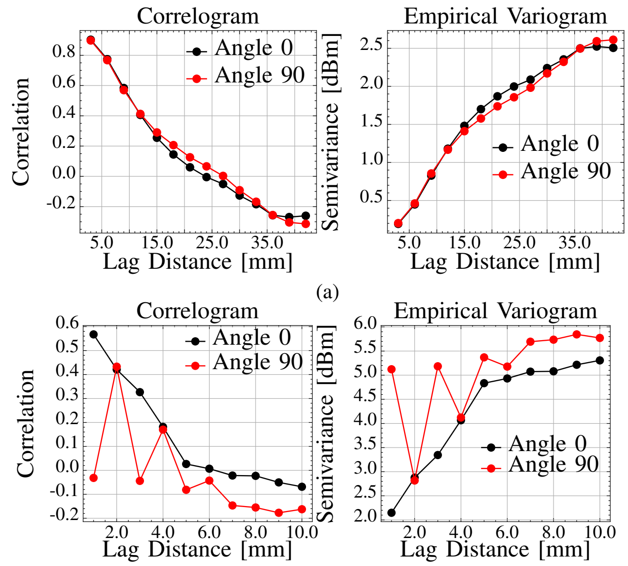

(a)

(b)

Figure 4.

Acknowledgments

The authors would like to thank Dr. Davide de Simone, from Politecnico di Milano, for providing the TI board, and Dr. Cheng Yang and Prof. Christian Schuster, both from Hamburg University of Technology, for their support in collecting the measurement data.

References

[1] W.-J. Zhao, E.-X. Liu, B. Wang, S.-P. Gao, and C. E. Png, "Differential evolutionary optimization of an equivalent dipole model for electromagnetic emission analysis," *IEEE Trans. Electromagn. Compat.*, vol. 60, no. 6, pp. 1635–1639, 2018.

[2] X. Wu, F. Grassi, G. Spadacini, S. A. Pignari, U. Paoletti, and I. Hoda, "Test design methodology for time-domain immunity investigations using electric near-field probes," *IEEE Trans. Electromagn. Compat.*, vol. 64, no. 3, pp. 603–612, 2022.

[3] D. Baudry, C. Arcambal, A. Louis, B. Mazari, and P. Eudeline, "Applications of the near-field techniques in emc investigations," *IEEE Trans. Electromagn. Compat.*, vol. 49, no. 3, pp. 485–493, 2007.

[4] X. Wu, F. Grassi, G. Spadacini, S. A. Pignari, U. Paoletti, and I. Hoda, "Investigation of semi-rigid coaxial test probes as rf injection devices for immunity tests at pcb level," *IEEE Access*, vol. 8, pp. 147 919–147 929, 2020.

[5] A. Plot, P. Besnier, and B. Azanowsky, "Efficient emc risk analysis of pcb using iterative surrogate-model enrichment and morris sensitivity analysis," in *2022 Int. Symp. Electromagn. Compat. – EMC Europe*, 2022, pp. 862–867.

[6] D. Deschrijver, F. Vanhee, D. Pissoort, and T. Dhaene, "Automated near-field scanning algorithm for the emc analysis of electronic devices," *IEEE Trans. Electromagn. Compat.*, vol. 54, pp. 502–503, 06 2012.

[7] C. E. Rasmussen and C. K. I. Williams, *Gaussian processes for machine learning.*, ser. Adaptive computation and machine learning. MIT Press, 2006.